East European Journal of Physics. 2. 251-259 (2026)
DOI:10.26565/2312-4334-2026-2-27 ISSN 2312-4334

MODELING THE IMPACT OF INCOMPLETE DOPANT IONIZATION ON BUILT-IN POTENTIAL AND C–V CHARACTERISTICS OF GaN p–n JUNCTIONS: A SCAPS-1D STUDY

Jo‘shqin Sh. Abdullayev[1,2]*, I.B. Sapaev[2], Jonibek Sh. Abdullayev[7], G.A. Abdikayimova[3], Sh.Sh. Akhmadaliev[4], M.M. Gulomova[5], Sh.O. Kholbekov[5], Kudrat Sh. Ruzmetov[6]

[1]*Institute of Fundamental and Applied Research, National Research University “TIIAME”, Tashkent 100000, Uzbekistan*
[2]*National Research University TIIAME, Department of Physics and Chemistry, Tashkent, Uzbekistan*
[3]*Tashkent State Technical University, Tashkent, Uzbekistan*
[4]*Fergana Medical Institute of Public Health, Fergana, Uzbekistan*
[5]*Karshi State Technical University, Karshi City, Kashkadaryo Region, Uzbekistan, 180100*
[6]*Tashkent State Agrarian University,100020, Tashkent, Uzbekistan*
[7]*Urgench State University, Hamid Olimjon Street, 14, Urgench, 220100 Uzbekistan*
**Corresponding Author e-mail: j.sh.abdullayev6@gmail.com*
Received January 27, 2026; revised April 14, 2026; accepted May 7, 2026

Incomplete dopant ionization in wide-bandgap semiconductors plays a critical role in determining carrier concentration, electrostatic properties, and overall device performance; however, its impact on GaN p–n junctions for optical photovoltaic converters (OPCs) remains insufficiently understood. In this work, SCAPS-1D simulations are employed to systematically investigate GaN p–n junctions incorporating three p-type acceptors (Mg, Zn, Be) and three n-type donors (Si, O, S) over doping concentrations of 10^{15}–10^{18} cm^{-3} and temperatures ranging from 77 K to 400 K. The temperature dependence of the bandgap is described by the Varshni relation ($R^2 = 0.9721$), while dopant ionization is modeled as a function of both temperature and doping level to capture its effects on carrier distribution, the built-in potential, and capacitance–voltage (C–V) characteristics. The results reveal a pronounced reduction in junction capacitance at lower temperatures due to incomplete acceptor ionization. For a representative doping level of 5×10^{17} cm^{-3}, the capacitance decreases from approximately 3.2 pF at 400 K to 1.5 pF at 77 K (≈53% reduction), primarily due to partial ionization of Mg acceptors, while donor species remain nearly fully ionized. These findings demonstrate that conventional models that neglect incomplete ionization significantly overestimate junction capacitance at low temperatures. Although the analysis is based on a one-dimensional framework, it provides physically consistent insight into the role of deep-level dopants and establishes a basis for future multidimensional TCAD investigations. This study highlights the necessity of incorporating incomplete-ionization effects into the design and optimization of high-efficiency, radiation-resilient GaN-based OPCs operating in extreme environments.
Keywords: *GaN; Dopant ionization; Incomplete ionization; Optical photovoltaic converters (OPCs); Temperature-dependent carrier activation; Capacitance–voltage characteristics; Built-in potential; Wide-bandgap (WBG); RF performance*
PACS: 73.40.Lq; 73.61.Cw; 73.61.Ey; 72.20.Jv; 84.60.Jt

INTRODUCTION

Wide-bandgap (WBG) semiconductors have emerged as enabling materials for next-generation power electronics and optoelectronic devices operating under extreme electrical, thermal, and radiation conditions [1–10]. Compared with conventional Si and GaAs, WBG materials—including GaN, 4H-SiC, β-Ga_2O_3, and diamond—offer significantly larger bandgaps, higher critical electric fields, superior thermal conductivity, and enhanced radiation tolerance, enabling reliable operation at elevated temperatures and high-power densities [1–10]. These properties make WBG semiconductors attractive for applications ranging from space-based solar energy systems and high-power laser energy transfer to radiation-hardened detectors and high-voltage electronics [4,9–14]. Among WBG materials, gallium nitride (GaN) has attracted significant attention due to its direct wide bandgap (3.39 eV), high breakdown field, and robust III–N bond strength, supporting stable operation under elevated temperatures and intense radiation [4,9,10,15,16]. Other WBG semiconductors, such as 4H-SiC (3.26 eV) and diamond (5.45 eV), also offer high breakdown voltages (3–10 MV/cm) and excellent thermal conductivity (~3.7 W/cm·K for SiC; ~2200 W/m·K for diamond), while β-Ga_2O_3 (~4.8 eV) exhibits ultrahigh theoretical breakdown limits, though challenges in dopant activation and thermal management remain [3,5,7,17–20].

Despite these advantages, incomplete dopant ionization remains a fundamental limitation in WBG semiconductors, particularly at low to moderate temperatures [21–25]. Deep dopant levels in combination with large bandgaps lead to substantial fractions of electrically inactive dopants, reducing free carrier concentration, increasing resistivity, and altering key device parameters. In GaN, p-type acceptors (Mg, Zn, Be) possess high activation energies (~120–160 meV), whereas n-type donors (Si, O, S) exhibit low activation energies (~20–32 meV). Similar incomplete ionization effects are observed in 4H-SiC (B, Al), diamond (B, P), and β-Ga_2O_3 (unintentional donors), highlighting the broad relevance of this phenomenon in WBG devices [3,5,7,22,23].

Incomplete ionization affects carrier density, built-in potential, depletion width, and capacitance-voltage (C–V) characteristics, which are critical for optical photovoltaic converters (OPCs) where carrier transport, recombination, and

Cite as: J.Sh. Abdullayev, I.B. Sapaev, J.Sh. Abdullayev, G.A. Abdikayimova, Sh.Sh. Akhmadaliev, M.M. Gulomova, Sh.O. Kholbekov, K.Sh. Ruzmetov, East Eur. J. Phys. 2, 251 (2026), https://doi.org/10.26565/2312-4334-2026-2-27
© J.Sh. Abdullayev, I.B. Sapaev, J.Sh. Abdullayev, G.A. Abdikayimova, Sh.Sh. Akhmadaliev, M.M. Gulomova, Sh.O. Kholbekov, K.Sh. Ruzmetov, 2026; CC BY 4.0 license

resistive losses determine efficiency [10,26]. GaN-based OPCs have achieved conversion efficiencies up to 79.6% at laser power densities of 10 W/cm², surpassing GaAs devices by over 10% [10,26,27]. However, their performance is highly sensitive to temperature-dependent ionization of deep acceptors, emphasizing the need for systematic evaluation. Radiation tolerance further underscores the importance of understanding dopant ionization, as GaN and III-nitride heterostructures (AlN/GaN, AlGaN/GaN, InAlN/GaN) maintain stable operation under high-dose proton, electron, neutron, and gamma irradiation [2,4,9,28]. Although extensive modeling has been conducted for WBG devices—including GaN/Si heterojunction solar cells [29], InGaN tandem cells [30], vertical GaN diodes [32-34], and AlGaN/GaN HEMTs [35–37] – few studies systematically investigate the effects of incomplete dopant ionization across realistic temperature and doping ranges. Existing research often neglects the influence of deep-level acceptors on C–V characteristics, built-in potential, and device efficiency.

In this study, we employ SCAPS-1D simulations to investigate GaN p–n junctions incorporating three p-type acceptors (Mg, Zn, Be) and three n-type donors (Si, O, S) across doping concentrations from 10^{15} to 10^{18} cm^{-3} and temperatures from 77 K to 400 K. The model accounts for the coupled influence of incomplete dopant ionization on carrier transport, recombination dynamics, and electrostatic behavior. Particular attention is given to the resulting variations in built-in potential, depletion width, and capacitance–voltage (C–V) characteristics, comparing cases with and without ionization effects.

It should be noted that, due to the inherent one-dimensional nature of SCAPS-1D, the present study focuses on capturing the fundamental trends associated with incomplete ionization rather than providing a fully comprehensive description of multidimensional device physics. Effects such as lateral field distribution, polarization-induced charges, and geometric non-uniformities—which are critical in realistic GaN-based structures—are beyond the scope of this approach. Nevertheless, the results provide physically meaningful insight into the role of deep-level dopants and establish a foundation for future investigations using advanced 2D/3D TCAD frameworks.

METHODS AND MATERIAL

2.1. Material Parameters, Doping, and Layer Structure

Gallium Nitride (GaN) is a III–V wide-bandgap semiconductor with a wurtzite crystal structure (a ≈ 3.189 Å, c ≈ 5.185 Å) and a direct bandgap of 3.39 eV at 300 K, making it highly suitable for high-power, high-frequency, and optoelectronic applications. For SCAPS-1D simulations, the electron effective mass is set to 0.20 m_0 and the hole effective masses to 1.0 m_0 (heavy) and 0.3 m_0 (light), corresponding to high electron mobility (~1500 cm²/V·s) and moderate hole mobility (~100 cm²/V·s). GaN exhibits a low intrinsic carrier concentration (~1×10^{-10} cm^{-3}), relative permittivity $\varepsilon \approx 9.5$, and a wide breakdown field (~3.3 MV/cm), enabling compact, high-voltage one-port capacitance (OPC) and RF designs. Its high thermal conductivity (~230 W/m·K) and melting point (~2500 °C) support reliable high-power operation, while strong optical absorption (~10^5 cm^{-1} at 3.4 eV) and radiation hardness make it suitable for advanced optoelectronic and space-based devices. Doping in SCAPS-1D was modeled using n-type donors (Si: 5×10^{17} cm^{-3}, O: 1×10^{16} cm^{-3}, S: 5×10^{16} cm^{-3}) with low activation energies (~20–32 meV) and p-type acceptors (Mg: 1×10^{18} cm^{-3}, Zn: 1×10^{17} cm^{-3}, Be: 5×10^{16} cm^{-3}) with higher activation energies (~120–160 meV). The incomplete ionization of acceptors in the p-GaN quasi-neutral region (QNR) reduces the effective hole concentration, significantly affecting the built-in potential, depletion width, and capacitance-voltage (C–V) characteristics.

The layer structure was defined with long quasi-neutral regions to accurately capture the junction behavior: the p-GaN layer was set to 2 µm and the n-GaN layer to 3–5 µm, ensuring that both QNRs were much thicker than the depletion region (~100–500 nm) calculated dynamically by SCAPS. Metallic ohmic contacts were applied at the device terminals to enable efficient carrier injection and extraction. To account for carrier dynamics and realistic device behavior, Shockley–Read–Hall (SRH) recombination was included with lifetimes $\tau_n = \tau_p$ = 1–10 ns and trap densities of 10^{13}–10^{15} cm^{-3}. This configuration allows simulation of frequency-dependent response, one-port capacitance (OPC), RF behavior, and high-power device reliability under both equilibrium and bias-dependent conditions.

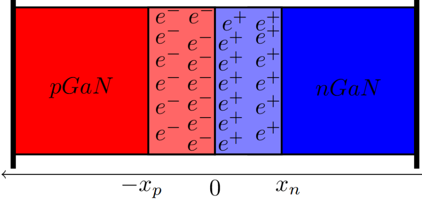

Figure 1. 2D schematic representation of the p–n GaN heterojunction simulated in SCAPS-1D

Figure 1 depicts a 2D schematic of the p–n GaN heterojunction simulated using SCAPS-1D, incorporating three acceptors (Mg, Zn, Be) in the p-type region and three donors (Si, O, S) in the n-type region. The p-GaN quasi-neutral region (QNR) is shown in red, with partially ionized acceptor ions due to their relatively high activation energies (~120–200 meV), whereas the n-GaN QNR is shown in blue with largely ionized donor ions (~20–32 meV). The depletion region at the junction is highlighted in light red on the p-side and light blue on the n-side, representing the space charge formed by ionized dopants. Metallic contacts are shown at the structure edges, and the positions $-x_p$, 0, and $-x_n$ correspond to the p-side depletion

boundary, metallurgical junction, and n-side depletion boundary, respectively. Electrons and holes indicate the distribution of mobile carriers. Near the junction $x = 0$, the electric field reaches its maximum, dominated by ionized dopants, while in the QNRs, the p-type region contains mostly neutral acceptors and the n-type region contains fully ionized donors. The distribution of ionized and neutral dopants in the GaN p–n junction reduces capacitance in C–V characteristics by altering effective carrier concentration, thereby affecting the built-in potential, depletion width, and frequency-dependent response. These effects critically impact RF performance, one-port capacitance (OPC), and device reliability, providing a clear physical basis for interpreting bias- and temperature-dependent behavior.

2.2 Numerical Modeling of Temperature-Dependent Ionization and Calibration

The temperature-dependent ionization of dopants in GaN p–n junctions was modeled numerically using SCAPS-1D, which allows the explicit incorporation of incomplete ionization effects for both acceptor and donor species. The p-type region included three acceptors (Mg, Zn, Be) with activation energies of 160 meV, 120 meV, and 150 meV, respectively, while the n-type region included three donors (Si, O, S) with activation energies of 20 meV, 32 meV, and 30 meV. This configuration reflects realistic doping conditions commonly employed in GaN-based optical photovoltaic converters (OPCs) and high-power devices. In SCAPS-1D, the fraction of ionized dopants $N_D^+(T)$ and $N_A^-(T)$ were calculated as a function of temperature using the Fermi–Dirac distribution (1a) and (1b):

$$\begin{cases} N_A^-(T) = \dfrac{N_A}{1 + \dfrac{g_A \cdot p_p(T)}{\beta_p(T) \cdot N_V(T)} \cdot \exp\left(\dfrac{\Delta E_A}{kT}\right)} & (1a) \\ N_D^+(T) = \dfrac{N_D}{1 + \dfrac{g_D \cdot n_n(T)}{\beta_n(T) \cdot N_C(T)} \cdot \exp\left(\dfrac{\Delta E_D}{kT}\right)} & (1b) \end{cases}$$

where N_D and N_A are the total donor and acceptor concentrations, E_D and E_A the dopant energy levels, E_F the Fermi level, k_B the Boltzmann constant, T the temperature, and g_D, g_A the dopant degeneracy factors.

This approach enables accurate modeling of partially ionized deep-level acceptors at cryogenic and moderate temperatures, which is particularly critical for p-GaN regions where Mg is the dominant dopant. To connect the quantum Fermi–Dirac statistics with classical Maxwell–Boltzmann approximations, temperature-dependent correction factors $\beta_n(T)$ and $\beta_p(T)$ are introduced. The numerical model was calibrated against reported experimental and simulation data for GaN p–n junctions [10,26,32], ensuring correct reproduction of key parameters such as built-in potential, depletion width, and capacitance-voltage (C–V) characteristics across the full temperature range. Both quasi-neutral regions and the depletion region were discretized with sufficient spatial resolution to capture sharp carrier and field gradients at the metallurgical junction. To isolate the impact of incomplete ionization, comparative simulations were conducted with full ionization assumed for all dopants. The resulting differences in carrier concentration, built-in potential, depletion width, and C–V response directly quantify the effect of deep-level acceptors and donors on junction performance. This calibrated model provides a reliable framework for predicting temperature- and doping-dependent behavior in GaN OPCs and other wide-bandgap devices operating under extreme conditions. The bandgap $E_g(T)$ typically decreases with increasing temperature due to lattice expansion and electron–phonon interactions. For GaN, this can be described using Varshni's empirical relation (2):

$$E_g(T) = E_g(0) - \frac{\alpha \cdot T^2}{T + \theta_D}. \quad (2)$$

Where: $E_g(0)$ is the bandgap at 0 K (~3.51 eV for GaN), α is the Varshni coefficient (~0.909 meV/K for GaN), θ_D is the Varshni temperature constant (~830 K for GaN), T is the absolute temperature in Kelvin.

The built-in potential V_{bi} is the equilibrium voltage established across a p–n junction due to diffusion of carriers, balancing drift and diffusion currents. In a GaN p–n junction, it depends on the doping concentrations and temperature, and is strongly influenced by incomplete ionization of deep-level dopants.

$$V_{bi}(T) = \frac{k_B \cdot T}{q} \cdot \ln\left(\frac{N_A \cdot N_D}{n_i^2(T)}\right). \quad (3)$$

The built-in potential V_{bi} of GaN p–n junctions was initially calculated using the classical expression (3). However, to accurately capture the effects of incomplete dopant ionization, this study employs the effective built-in potential $V_{bi,eff}$ as defined in expression (4), which incorporates the temperature-dependent fraction of ionized acceptors and donors in both p- and n-type regions.

$$V_{bi,eff}(T) = \frac{k_B \cdot T}{q} \cdot \ln\left(\frac{N_A^+(T) \cdot N_D^+(T)}{n_i^2(T)}\right). \quad (4)$$

Temperature controls dopant ionization, thereby affecting carrier concentration, depletion width, and built-in potential, which together determine the junction capacitance. In GaN, deep acceptors lead to reduced capacitance at low temperatures, while higher temperatures increase ionization and capacitance, critically influencing C–V behavior and device performance.

$$C_{p-n} = S \cdot \sqrt{\frac{q \cdot \varepsilon \cdot \varepsilon_0 \cdot N_A \cdot N_D}{2 \cdot (N_A + N_D) \cdot (V_{bi}(T) - V_{p-n})}} \tag{5}$$

Although many previous studies [25–30] evaluate junction capacitance using the classical approach (5), in the present work, the capacitance is calculated by explicitly incorporating the temperature- and doping-dependent ionized dopant concentrations from expressions (1a) and (1b), together with the effective built-in potential from expression (4), as formulated in expression (6).

$$C_{p-n} = S \cdot \sqrt{\frac{q \cdot \varepsilon \cdot \varepsilon_0 \cdot N_A \cdot N_D}{2 \cdot \left(N_D \cdot \left(1 + \frac{g_A \cdot p_p(T)}{\beta_p(T) \cdot N_V(T)} \cdot \exp\left(\frac{\Delta E_A}{kT} \right) \right) + N_A \cdot \left(1 + \frac{g_D \cdot n_n(T)}{\beta_n(T) \cdot N_C(T)} \cdot \exp\left(\frac{\Delta E_D}{kT} \right) \right) \right) \cdot \left(V_{bi,eff}(T) - V_{p-n} \right)}} \tag{6}$$

Figure 2. Calibration of GaN bandgap versus temperature.

The temperature-dependent bandgap of GaN was modeled using the Varshni equation over 77–400 K, with experimental calibration points in the 200–400 K range. The fitted parameters, Eg(0) = 3.51 eV, α = 0.00091 eV/K, and θ_D = 630 K, yield a coefficient of determination $R^2 = 0.9721$, demonstrating excellent agreement between the model and experimental data [39,40]. The results indicate an approximately linear decrease of $E_g$below 300 K, with pronounced nonlinear behavior at higher temperatures. This temperature dependence directly affects carrier generation, built-in potential, and junction capacitance in GaN-based optical photovoltaic converters (OPCs), emphasizing the necessity of incorporating accurate $E_g(T)$models in device simulations to optimize performance under high-temperature and high-efficiency operating conditions.

RESULTS AND DISCUSSION

The ionization behavior of acceptor (Mg, Zn, Be) and donor (Si, O, S) dopants in lightly doped GaN (NA = ND = 1×10^{15} cm^{-3}) exhibits strong temperature dependence, with pronounced freeze-out effects at cryogenic temperatures and nearly complete activation above room temperature. At temperatures below 50 K, dopants with high activation energies, such as Mg and Be, remain mostly inactive (ionization fraction $P < 0.1$), whereas dopants with lower activation energies, like Zn and Si, begin ionizing at higher rates, demonstrating the sensitivity of carrier activation to dopant energy levels. In the intermediate range of 77–150 K, the ionization fraction rises sharply, with donor species generally activating at lower temperatures than acceptors due to their smaller activation energies, higher degeneracy, and the larger conduction-band density of states. Mapping the ionization across temperature and dopant concentration shows that low dopant densities intensify freeze-out, while higher concentrations partially reduce incomplete ionization, although significant suppression remains at cryogenic temperatures even for N ~ 10^{18} cm^{-3}. These results underline the importance of dopant choice in GaN devices, particularly for low-temperature and high-power applications. Low-activation-energy donors such as Si and S provide stable electron conduction in n-type layers, whereas careful selection and co-doping of acceptors (Mg, Zn) is required to enhance hole densities in p-type layers. Incorporating temperature-dependent effective densities of states and incomplete ionization effects into device simulations is crucial for accurate prediction of carrier concentration, depletion widths, and current transport. From a design perspective, this understanding aids in optimizing high-power electronics, LEDs, HEMTs, and GaN-based optical photovoltaic converters, ensuring reliable operation across 77–400 K and supporting applications ranging from high-temperature operation to cryogenic devices such as sensors, quantum technologies, and low-noise photodetectors.

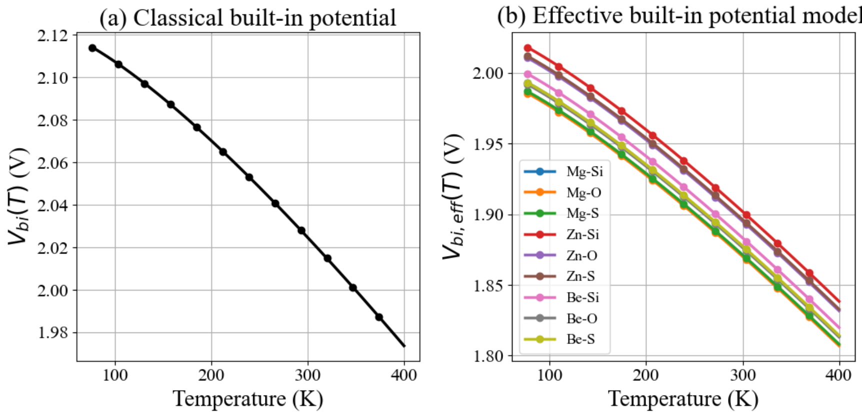

Figure 3. Temperature-dependent built-in potential of GaN p–n junctions: (a) classical model assuming complete dopant ionization; (b) effective model including temperature-dependent incomplete ionization of Mg, Zn, Be acceptors and Si, O, S donors

Figure 3(a) presents the temperature dependence of the built-in potential $V_{bi}$of a GaN p–n junction calculated using the classical expression, which assumes complete ionization of dopants. Under this assumption, V_{bi}increases monotonically with temperature due to the $\frac{k_BT}{q}$ prefactor and the strong temperature dependence of the intrinsic carrier concentration $n_i(T)$. For the considered doping levels ($N_A = N_D = 5 \times 10^{17}$ cm^{-3}), the classical model predicts V_{bi}values of approximately 3.15 V at 77 K, decreasing slightly to ~3.05 V at 300 K and ~2.95 V at 400 K. This smooth variation reflects only intrinsic semiconductor properties and neglects the reduced electrical activity of deep dopants at low and intermediate temperatures. In contrast, Figure 3(b) illustrates the effective built-in potential $V_{bi,\text{eff}}$obtained by explicitly accounting for incomplete dopant ionization through temperature-dependent ionized acceptor and donor concentrations. At low temperatures, the impact of incomplete ionization is pronounced, particularly for Mg-doped p-type GaN with an activation energy of 160 meV. For example, at 77 K, $V_{bi,\text{eff}}$ for the Mg–Si junction is reduced by more than 0.4–0.6 V relative to the classical prediction, corresponding to a reduction of ~15–20%. As the temperature increases, thermal activation progressively ionizes both acceptors and donors, leading to a gradual increase in $V_{bi,\text{eff}}$. Above ~300 K, the effective built-in potentials for all dopant combinations (Mg–Si, Zn–Si, Be–Si, and corresponding O and S donors) converge toward the classical V_{bi}, with deviations below 5 % at 400 K.

A clear hierarchy among acceptors is observed: Zn-doped GaN (120 meV) exhibits the highest $V_{bi,\text{eff}}$at low temperatures, followed by Be (150 meV), while Mg shows the strongest suppression due to its deeper acceptor level. Donor choice (Si, O, S) introduces smaller variations (<0.1–0.15 V across the full temperature range), consistent with their relatively shallow activation energies (20–32 meV). These results demonstrate that p-type dopant activation dominates the deviation from the classical model in GaN p–n junctions.

From a device-physics perspective, the reduced $V_{bi,\text{eff}}$ at low temperatures implies wider depletion regions and lower junction capacitance than predicted by classical theory, directly affecting C–V characteristics, RF response, and carrier collection efficiency. This is particularly relevant for GaN-based optical photovoltaic converters (OPCs) and space or cryogenic applications, where devices may operate well below room temperature. The comparison between Figures 3(a) and 3(b) highlights the necessity of incorporating incomplete ionization in quantitative modeling of wide-bandgap devices. Future work should extend this framework to non-uniform doping profiles, polarization-induced charges in III-nitride heterostructures, and high-field operation, as well as experimental validation through temperature-dependent C-V and I–V measurements. Such integrated modeling will be essential for predictive design of high-efficiency, radiation-hard GaN devices operating under extreme thermal conditions.

Figure 4 illustrates the strong asymmetry between acceptor and donor ionization in GaN as a function of temperature and doping concentration. As shown in Fig. 4(a), deep acceptors (Mg, Zn, Be) exhibit severe incomplete ionization, particularly at low temperatures and high doping densities. Magnesium, with an activation energy of 160 meV, is the most affected: at 300 K and $N_A \sim 10^{17}$–10^{18} cm^{-3}, only ~10–15 % of Mg atoms are ionized, while below 50 K Mg is almost completely frozen out. Even at elevated temperatures (~400 K), full activation is not achieved, highlighting the intrinsic limitation of p-type GaN. Lower-activation-energy acceptors partially mitigate this effect; at 300 K, Zn (120 meV) and Be (150 meV) reach ionization fractions of ~75 % and ~65 %, respectively, demonstrating improved but still incomplete hole activation. In contrast, Fig. 4(b) shows that n-type donors in GaN are nearly fully ionized across the entire investigated temperature range. Silicon donors (20 meV) exhibit ~85 % ionization already at ~10 K and exceed 99 % ionization at room temperature, with oxygen (32 meV) and sulfur (30 meV) showing similarly high activation (>95 % at 300 K). Donor ionization remains largely insensitive to both temperature and doping concentration, ensuring stable electron densities from cryogenic to high-temperature operation. These results confirm that incomplete ionization is the dominant limitation of p-type GaN and directly governs the built-in potential, depletion width, and capacitance–voltage behavior of GaN p–n junctions. For GaN-based optical photovoltaic converters and high-power devices, the reduced hole density due to incomplete Mg activation increases series resistance, degrades carrier collection, and reduces efficiency,

whereas the fully ionized n-type region ensures robust electron transport. Accurate inclusion of temperature- and concentration-dependent dopant ionization is therefore essential for realistic modeling and optimization of GaN devices operating over the 4–400 K range.

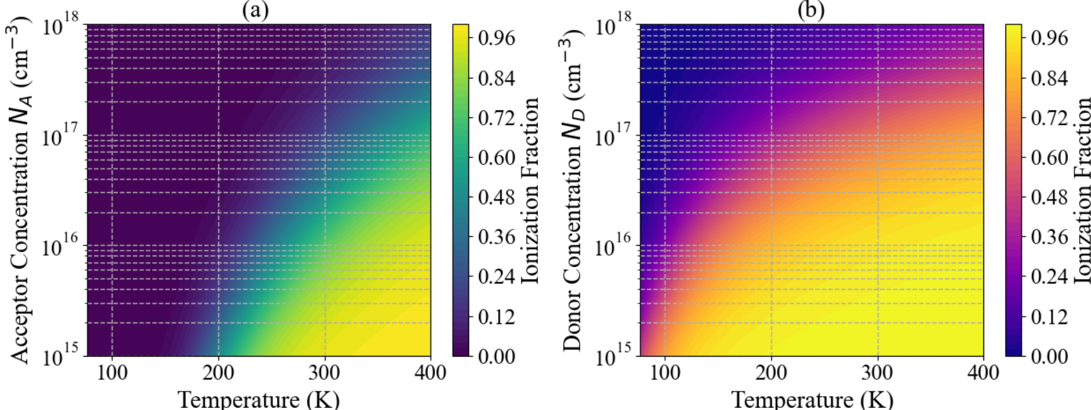

Figure 4. Temperature- and concentration-dependent ionization probabilities of dopants in GaN.
(a) Acceptor ionization probability $P_A(T)$for Mg, Zn, and Be over 77–400 K and 10^{14}–10^{18} cm^{-3}, (b) Donor ionization probability $P_D(T, N_D)$for Si, O, and S over the same temperature and concentration ranges.

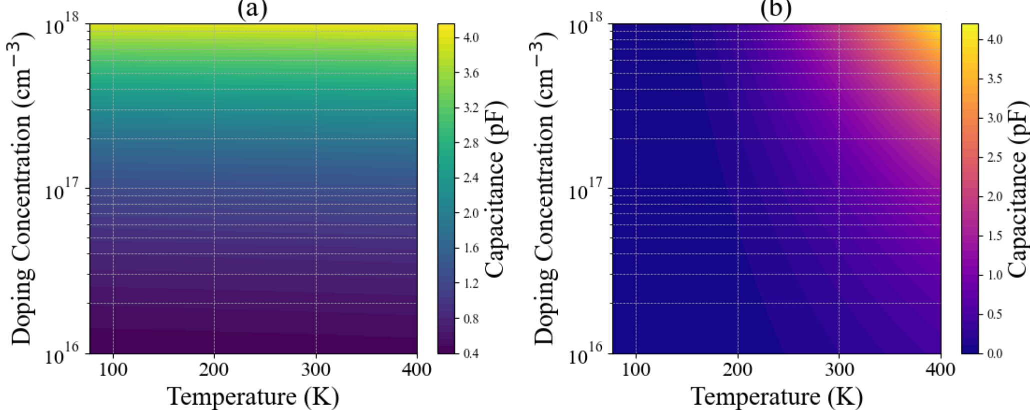

Figure 5. Temperature- and doping-dependent p–n junction capacitance of GaN: (a) classical model assuming full dopant ionization, and (b) effective model accounting for incomplete ionization of Mg acceptors and Si donors, highlighting reduced capacitance at low temperatures and high doping

Temperature- and doping-dependent junction capacitance in GaN. Figure 5 illustrates the calculated p–n junction capacitance of GaN as a function of temperature (77–400 K) and doping concentration (10^{16}–10^{18} cm^{-3}). Figure 5(a) presents the classical capacitance assuming complete dopant ionization, while Figure 5(b) accounts for the incomplete ionization of Mg acceptors (E_A = 160 meV) and Si donors (E_D = 20 meV). In the classical model (Figure 5(a)), the capacitance increases monotonically with doping, reaching up to ~4.5 pF at the highest doping ($N_A = N_D = 10^{18}$ cm^{-3}). Temperature dependence is relatively weak, with $C_{p\text{–}n}$ decreasing slightly at higher temperatures due to the increase in intrinsic carrier concentration and the logarithmic dependence of the built-in potential $V_{bi}(T)$. Across the full temperature range, the variation in capacitance for mid-range doping ($N_A= N_D = 10^{17}$ cm^{-3}) is only ~5%, indicating negligible temperature sensitivity under full ionization assumptions. In contrast, the effective capacitance model (Figure 5(b)) shows a pronounced reduction at low temperatures due to incomplete ionization of Mg. For a typical p-type doping of 5×10^{17} cm^{-3} and n-type doping of 5×10^{17} cm^{-3}, the capacitance drops from ~3.2 pF at 400 K to ~1.5 pF at 77 K, highlighting a ~53% reduction caused by the freeze-out of acceptors. Donor ionization remains nearly complete across the temperature range, so the observed decrease is primarily driven by Mg acceptors. The impact of incomplete ionization is most significant at high doping levels ($N_A \geq 10^{18}$ cm^{-3}), where the capacitance reduction reaches ~60% at cryogenic temperatures. These results emphasize that classical capacitance models overestimate $C_{p\text{–}n}$ at low temperatures, particularly for heavily Mg-doped p-type GaN. The effective model demonstrates that incomplete ionization must be incorporated to accurately predict junction behavior, especially for optical photovoltaic converters, high-power LEDs, and high-voltage GaN devices operating below room temperature. Overall, Figure 5 highlights the asymmetry between acceptor and donor ionization: n-type regions maintain robust capacitance due to nearly complete Si ionization, while p-type regions exhibit strong temperature-dependent reductions in capacitance. This behavior directly impacts depletion width, junction voltage, and charge storage, reinforcing the necessity of including temperature- and dopant-dependent ionization effects in GaN device simulations.

CONCLUSIONS

This study quantitatively demonstrates the critical impact of incomplete dopant ionization on the electrostatic and capacitance–voltage (C–V) characteristics of GaN p–n junctions using SCAPS-1D simulations. The analysis was carried out over doping concentrations ranging from 10^{15} to 10^{18} cm^{-3} and temperatures between 77 K and 400 K, incorporating both deep acceptors (Mg, Zn, Be) and shallow donors (Si, O, S).

The results show that incomplete ionization of deep acceptors, particularly Mg with activation energies of approximately 120–160 meV, leads to significant carrier freeze-out at low temperatures. For a representative doping level of 5×10^{17} cm^{-3}, the junction capacitance decreases from about 3.2 pF at 400 K to 1.5 pF at 77 K, corresponding to a reduction of approximately 53%. In more extreme cases, the overall reduction in capacitance can reach ~60% at cryogenic temperatures. This reduction is accompanied by a decrease in the built-in potential and an increase in the depletion width due to the reduced free-hole concentration.

In contrast, n-type donors with lower activation energies (~20–32 meV) remain nearly fully ionized across the entire temperature range (77–400 K), showing minimal impact on carrier availability. The bandgap variation modeled using the Varshni relation exhibits strong agreement ($R^2 = 0.9721$), ensuring accurate temperature-dependent simulation results.

Importantly, conventional models that neglect incomplete ionization significantly overestimate junction capacitance, particularly in heavily Mg-doped structures (≥10^{17} cm^{-3}). This leads to inaccuracies in predicting device performance, especially for applications operating under low-temperature or high-radiation conditions.

Although the study is limited to a one-dimensional SCAPS-1D framework, it captures the essential physical trends and provides reliable insight into the role of dopant ionization. The findings clearly indicate that incorporating temperature- and doping-dependent ionization effects is essential for accurate modeling and optimization of GaN-based optical photovoltaic converters, which have demonstrated efficiencies up to 79.6% at 10 W/cm², as well as for high-power and radiation-resilient electronic devices operating across extreme environments.

ORCID

Jo‘shqin Sh. Abdullayev, https://orcid.org/0000-0001-6110-6616; **I.B. Sapaev,** https://orcid.org/0000-0003-2365-1554; **Jonibek Sh. Abdullayev,** https://orcid.org/0000-0001-8950-2135; **G.A. Abdikayimova,** https://orcid.org/0000-0003-3739-8430; **Kudrat Sh. Ruzmetov,** https://orcid.org/0009-0002-2575-6827; **Sh.Sh. Akhmadaliev,** https://orcid.org/0000-0003-4830-2887

REFERENCES

[1] T. Maeda, T. Narita, S. Yamada, T. Kachi, T. Kimoto, M. Horita, and J. Suda, “Impact ionization coefficients and critical electric field in GaN,” Journal of Applied Physics, **129**(18), 185702 (2021). https://doi.org/10.1063/5.0050793

[2] S.J. Pearton, R. Deist, F. Ren, L. Liu, A.Y. Polyakov, and J. Kim, “Review of radiation damage in GaN-based materials and devices,” Journal of Vacuum Science and Technology A, **31**(5), 050801 (2013). https://doi.org/10.1116/1.4799504

[3] N. Donato, and F. Udrea, “Static and dynamic effects of the incomplete ionization in superjunction devices,” IEEE Transactions on Electron Devices, **65**(10), 4469–4475 (2018). https://doi.org/10.1109/TED.2018.2867058

[4] S.J. Pearton, Y.-S. Hwang, and F. Ren, “Radiation effects in GaN-based high electron mobility transistors,” Journal of Materials, **67**, 1601–1611 (2015). https://doi.org/10.1007/s11837-015-1401-2

[5] A.T. Neal, S. Mou, R. Lopez, J.V. Li, D.B. Thomson, K.D. Chabak, and G.H. Jessen, “Incomplete ionization of a 110 meV unintentional donor in β-Ga_2O_3 and its effect on power devices,” Scientific Reports, **7**, 13218 (2017). https://doi.org/10.1038/s41598-017-13341-8

[6] J.Sh. Abdullayev, and I.B. Sapaev, “Factors influencing the ideality factor of semiconductor p-n and p-i-n junction structures at cryogenic temperatures,” East European Journal of Physics, (4), 329–333 (2024). https://doi.org/10.26565/2312-4334-2024-4-37

[7] M. Phifer, S. Hossain, J. Osborne, Z. Xie, and M. Alam, “Demonstration of TCAD modeling for GaN devices,” in: *SoutheastCon. 2025*, (IEEE, 2025), pp. 1–6. https://doi.org/10.1109/SoutheastCon56624.2025.10971621

[8] H. Shang, and Y. Jiang, “A physical model of a diamond vertical Schottky diode including incomplete ionization and thermal effects,” Journal of Physics D: Applied Physics, **58**(15), 155104 (2025). https://doi.org/10.1088/1361-6463/adb9fb

[9] C. Onwukaeme, and H.-Y. Ryu, “Design of GaN-based laser diode structures with nonuniform doping distribution in a p-AlGaN cladding layer for high-efficiency operation,” Crystals, **15**(3), 259 (2025). https://doi.org/10.3390/cryst15030259

[10] J. Wei, J. Hao, Q. Zhao, J. Fan, F. Zhang, and Z. Dong, “Comparative study of wide-bandgap materials for neutron detection: GaN and 4H-SiC,” Nuclear Technology, **211**(12), 3080–3093 (2025). https://doi.org/10.1080/00295450.2025.2462444

[11] J.F. Lozano, N. Seoane, J.M. Guedes, E. Comesaña, J.G. Fernandez, F.M. Almonacid, E.F. Fernández, and A. García-Loureiro, “Gallium nitride: A strong candidate to replace GaAs as base material for optical photovoltaic converters in space exploration,” Optics and Laser Technology, **192**(Part A), 113447 (2025). https://doi.org/10.1016/j.optlastec.2025.113447

[12] J.Sh. Abdullayev, “Influence of linear doping profiles on the electrophysical features of p-n junctions. East European Journal of Physics, (1), 245–249 (2025). https://doi.org/10.26565/2312-4334-2025-1-26

[13] J.Sh. Abdullayev, and I.B. Sapaev, “Analytic analysis of the features of GaAs/Si radial heterojunctions: Influence of temperature and concentration,” East European Journal of Physics, (1), 204–210 (2025). https://doi.org/10.26565/2312-4334-2025-1-21

[14] J.Sh. Abdullayev, I.B. Sapaev, N. Esanmuradova, S. Kadirov, and S. Kuliyev, “Mathematical analysis of the features of radial p-n junction: Influence of temperature and concentration,” East European Journal of Physics, (2), 220–225 (2025). https://doi.org/10.26565/2312-4334-2025-2-24

[15] S. Chatterjee, and M. Mukherjee, “Electrical Characterization in Ultra-Wide Band Gap III-Nitride Heterostructure IMPATT/HEMATT Diodes: A Room-Temperature Sub-Millimeter Wave Power Source,” J. Electron. Mater. **52**, 1552–1563 (2023). https://doi.org/10.1007/s11664-022-10090-2

[16] J.Sh. Abdullayev, I.B. Sapaev, and S.R. Kadirov, The role of recombination types in efficiency limits of radial p-n junctions based on Si and GaAs. East European Journal of Physics, (2), 252–257 (2025). https://doi.org/10.26565/2312-4334-2025-2-30

[17] J.Sh. Abdullayev, I.B. Sapaev, J.S. Abdullayev, D.A. Juraev, M.J. Jalalov, and E.E. Elsayed, “Mathematical Modeling of Incomplete Ionization in Radial *p*-Si/*n*-GaAs Heterojunctions: Temperature and Doping Effects. *J. Electron. Mater.* **54**, 10484–10492 (2025). https://doi.org/10.1007/s11664-025-12391-8

[18] J.Sh. Abdullayev, L. Abdullayeva, L. Agamalieva, and R. Ismailova, "Correlating Ni microstructure with Schottky barrier homogeneity in monolayer MoS_2 field-effect transistors," Advanced Physical Research, **7**(3), 350–357 (2025). https://doi.org/10.62476/apr.73350
[19] P. Murugapandiyan, K. Sri Rama Krishna, A. Revathy, and A. Fletcher, "Enhancement Mode AlGaN/GaN MISHEMT on Ultra-Wide Band Gap β-Ga_2O_3 Substrate for RF and Power Electronics," J. Electron. Mater. **53**, 2973–2987 (2024). https://doi.org/10.1007/s11664-024-11005-z
[20] J.S. Abdullayev, D.A. Qalandarova, M.S. Ibragimova, I.B. Sapaev, and J.I. Razzokov, "Experimental and Simulation-Based Investigation of p-Si/n-CdS Heterojunctions: From Cryogenic Freeze-Out to Room Temperature Operation," J. Electron. Mater. **55**, 2229–2239 (2026). https://doi.org/10.1007/s11664-025-12642-8
[21] A. Kumar, G. Kumar, and C. Kumar, "Design and Performance Evaluation of a $Ge_{1-x}Sn_x$/Ge Multiple Quantum Well Heterojunction Phototransistor for Long-Haul DWDM Optical Communication Systems," J. Electron. Mater. (2026). https://doi.org/10.1007/s11664-025-12653-5
[22] M.A.A. Rosle, and M.Z. Pakhuruddin, "Investigation of gallium nitride emitter thickness in GaN/Si heterojunction solar cell by SCAPS-1D," NanoVol, **20**(09), 2550026 (2025). https://doi.org/10.1142/S1793292025500262
[23] M.K. Omar, M. Rashid, and M.Z. Pakhuruddin, "Investigation on indium concentration in two-terminal tandem indium gallium nitride solar cells by SCAPS-1D," Physica Scripta, **99**(11), 115531 (2024). https://doi.org/10.1088/1402-4896/ad8193
[24] H. Abboudi, W. Belaid, R. En-nadir, I. Ez-zejjari, M. Zouini, A. Sali, and H. El Ghazi, "Optimization of $In_xGa_{1-x}N$ P-I-N solar cells: Achieving 21% efficiency through SCAPS-1D modeling," Crystals, **15**(7), 633 (2025). https://doi.org/10.3390/cryst15070633
[25] Z. Hu, K. Nomoto, B. Song, M. Zhu, M. Qi, M. Pan, X. Gao, *et al.*, "Near unity ideality factor and Shockley-Read-Hall lifetime in GaN-on-GaN p-n diodes with avalanche breakdown featured," Applied Physics Letters, **107**(24), 243501 (2015). https://doi.org/10.1063/1.4937436
[26] J.S. Abdullayev, M.S. Ibragimova, J.Sh. Abdullayev, and I.B. Sapaev, "Cryogenic material and electrophysical changes in Si and GaAs," East European Journal of Physics, (1), 343–350 (2026). https://doi.org/10.26565/2312-4334-2026-1-40
[27] Y.-C. Lai, Y.-N. Zhong, M.-Y. Tsai, and Y.-M. Hsin, "Gate capacitance and off-state characteristics of E-mode p-GaN gate AlGaN/GaN high-electron-mobility transistors after gate stress bias," Journal of Electronic Materials, **50**, 1162–1166 (2021). https://doi.org/10.1007/s11664-020-08949-1
[28] N. Bano, I. Hussain, E.A. Al-Ghamdi, and M.S. Ahmad, "Quantitative analysis of electrically active defects in Au/AlGaN/GaN HEMTs structure using capacitance–frequency and DLTS measurements," Journal of Physics Communications, **5**(12), 125010 (2021). https://doi.org/10.1088/2399-6528/ac41aa
[29] S. Lv, S. Wang, J. Yu, G. Tian, G. Wang, P. An, K. Song, *et al.*, "Wafer scale gallium nitride integrated electrode toward robust high temperature energy storage," Small, **20**(27), 2310837 (2024). https://doi.org/10.1002/smll.202310837
[30] W. Yang, J.-S. Yuan, B. Krishnan, A.J. Tzou, and W.-K. Yeh, "C-V measurement under different frequencies and pulse-mode voltage stress to reveal shallow and deep trap effects of GaN HEMTs," in: *2018 IEEE 6th Workshop on Wide Bandgap Power Devices and Applications (WiPDA)*, (Atlanta, GA, USA, 2018). https://doi.org/10.1109/WIPDA.2018.8569206
[31] J. Park, S.H. Lee, I.M. Kang, and Y.J. Yoon, "Fabrication of AlGaN/GaN HEMT using TMAH pre-treatment and analysis of electrical characteristics by proton irradiation," Current Applied Physics, **75**, 33–39 (2025). https://doi.org/10.1016/j.cap.2025.04.010
[32] H. Sun, Q. Fan, X. Ni, Q. Luo, and X. Gu, "Low-pressure chemical vapor deposition SiNx process study and its impact on interface characteristics of AlGaN/GaN MISHEMTs," Micromachines, **16**(4), 442 (2025). https://doi.org/10.3390/mi16040442
[33] D.A. Qalandarova, M.S. Ibragimova, J.S. Abdullayev, and I.B. Sapaev, "Mathematical modeling of electrostatic potential in radial and planar p–n junctions: A comparative study," East European Journal of Physics, (1), 333–342 (2026). https://doi.org/10.26565/2312-4334-2026-1-39
[34] J.S. Abdullayev, M.S. Ibragimova, J.Sh. Abdullayev, and I.B. Sapaev, "Thermal expansion characteristics of planar and radial Si/GaAs p–n heterojunctions," East European Journal of Physics, (1), 388–395 (2026). https://doi.org/10.26565/2312-4334-2026-1-46
[35] H. Teisseyre, P. Perlin, T. Suski, I. Grzegory, S. Porowski, J. Jun, A. Pietraszko, and T.D. Moustakas, "Temperature dependence of the energy gap in GaN bulk single crystals and epitaxial layer," Journal of Applied Physics, **76**(4), 2429–2434 (1994). https://doi.org/10.1063/1.357592
[36] C. Prall, M. Ruebesam, C. Weber, M. Reufer, and D. Rueter, "Photoluminescence from GaN layers at high temperatures as a candidate for in situ monitoring in MOVPE," Journal of Crystal Growth, **397**, 24–28 (2014). https://doi.org/10.1016/j.jcrysgro.2014.04.001
[37] J.Sh. Abdullayev, D.A. Qalandarova, and M.Sh. Ibragimova, "Impact of incomplete ionization on the critical electric field of p-n junction structures based on Si and GaAs," Low Temperature Physics, **52**(2), 164–169 (2026). https://doi.org/10.1063/10.0042291

МОДЕЛЮВАННЯ ВПЛИВУ НЕПОВНОЇ ІОНІЗАЦІЇ ДОМІШОК НА ВБУДОВАНИЙ ПОТЕНЦІАЛ І ВОЛЬТ-ФАРАДНІ (C–V) ХАРАКТЕРИСТИКИ p–n ПЕРЕХОДІВ GaN: ДОСЛІДЖЕННЯ ЗА ДОПОМОГОЮ SCAPS-1D

Джошкін Ш. Абдуллаєв[2], І.Б. Сапаєв[2], Джонібек Ш. Абдуллаєв[7], Г.А. Абдикаїмова[3], Ш.Ш. Ахмадалієв[4], М.М. Гуломова[5], Ш.О. Холбеков[5], Кудрат Ш. Рузметов[6]
[1]*Інститут фундаментальних та прикладних досліджень, Національний дослідницький університет «TIIAME», Ташкент 100000, Узбекистан*
[2]*Національний дослідницький університет TIIAME, фізико-хімічний факультет, Ташкент, Узбекистан*
[3]*Ташкентський державний технічний університет, Ташкент, Узбекистан*
[4]*Ферганський медичний інститут громадського здоров'я, Фергана, Узбекистан*
[5]*Каршинський державний технічний університет, місто Карші, Кашкадарьинська область, Узбекистан, 180100*
[6]*Ташкентський державний аграрний університет, 100020, Ташкент, Узбекистан*
[7]*Ургенчський державний університет, вул. Хаміда Олімжона, 14, Ургенч, 220100 Узбекистан*

Неповна іонізація домішок у напівпровідниках із широкою забороненою зоною відіграє критичну роль у визначенні концентрації носіїв заряду, електростатичних властивостей і загальної продуктивності пристроїв; однак її вплив на p–n переходи GaN для оптичних фотовольтаїчних перетворювачів (OPC) залишається недостатньо вивченим. У цій роботі використано моделювання SCAPS-1D для систематичного дослідження p–n переходів GaN із трьома p-типовими акцепторами

(Mg, Zn, Be) і трьома n-типовими донорами (Si, O, S) у діапазоні концентрацій легування 10^{15}–10^{18} см$^{-3}$ і температур від 77 K до 400 K. Температурна залежність ширини забороненої зони описується за допомогою співвідношення Варшні ($R^2 = 0{,}9721$), тоді як іонізація домішок моделюється як функція температури та рівня легування для врахування її впливу на розподіл носіїв, вбудований потенціал і вольт-фарадні (C–V) характеристики. Результати демонструють суттєве зменшення ємності переходу за нижчих температур через неповну іонізацію акцепторів. Для характерного рівня легування 5×10^{17} см$^{-3}$ ємність зменшується приблизно з 3,2 пФ при 400 K до 1,5 пФ при 77 K (≈53% зниження), що переважно зумовлено частковою іонізацією акцепторів Mg, тоді як донорні домішки залишаються майже повністю іонізованими. Ці результати показують, що традиційні моделі, які ігнорують неповну іонізацію, суттєво переоцінюють ємність переходу за низьких температур. Хоча аналіз базується на одновимірній моделі, він надає фізично узгоджене розуміння ролі глибоких домішкових рівнів і закладає основу для майбутніх багатовимірних TCAD-досліджень. Це дослідження підкреслює необхідність урахування ефектів неповної іонізації під час проєктування та оптимізації високоефективних, стійких до радіації OPC на основі GaN, що працюють в екстремальних умовах.
Ключові слова: *GaN; іонізація домішок; неповна іонізація; оптичні фотовольтаїчні перетворювачі (OPC); температурно-залежна активація носіїв; вольт-фарадні характеристики; вбудований потенціал; широкозонні напівпровідники (WBG); радіочастотні характеристики*